Noise performance of high-efficiency germanium quantum dot photodetectors

Stylianos Siontas,[1,a)] Pei Liu,[2,a)] Alexander Zaslavsky,[2] and Domenico Pacifici[1,b)]
[1]School of Engineering, Brown University, 184 Hope St., Providence, Rhode Island 02912, USA
[2]Department of Physics and School of Engineering, Brown University, 182–184 Hope St., Providence, Rhode Island 02912, USA

(Received 9 June 2016; accepted 26 July 2016; published online 4 August 2016)

We report on the noise analysis of high performance germanium quantum dot (Ge QD) photodetectors with responsivity up to ~2 A/W and internal quantum efficiency up to ~400%, over the 400–1100 nm wavelength range and at a reverse bias of −10 V. Photolithography was performed to define variable active-area devices that show suppressed dark current, leading to a higher signal-to-noise ratio, up to 10^5, and specific detectivity $D^* \simeq 6 \times 10^{12}$ cm Hz $^{1/2}$ W^{-1}. These figures of merit suggest Ge QDs as a promising alternative material for high-performance photodetectors working in the visible to near-infrared spectral range. *Published by AIP Publishing.* [http://dx.doi.org/10.1063/1.4960532]

Efficient and fast photodetectors (PDs) are crucial components of integrated optoelectronic circuits. Because of its small bandgap, crystalline germanium (Ge) has become a popular PD material for near-infrared photodetectors.[1–4] Various forms of nanostructured Ge have been investigated for improved optoelectronic performance,[4–10] including Ge quantum dots (QDs) embedded in an oxide matrix for high-efficiency photodetection.[5,10–15] In this letter, we perform photoresponse characterization as well as noise analysis of metal-oxide-semiconductor (MOS) PDs based on Ge QDs embedded in an oxide matrix. A 200 nm-thick oxide film containing Ge QDs was fabricated by co-sputtering of Ge and SiO_2 targets on *n*-Si substrates held at a temperature of 400 °C during the deposition.[16,17] In addition, a 500 °C annealing step was performed in a N_2 environment for 30 min to improve the quality of the oxide matrix while generating a higher density of crystalline Ge QDs with larger size.[13] Subsequently, an optically transparent, highly conductive ~100 nm-thick ITO layer was grown as the top gate electrode using sputter deposition through a ~0.25 cm^2 shadow mask. The sample was then cleaved to define a device with active area of ~1.5 mm^2. Finally, photolithography was performed on the remaining part of the sample to define several devices with 0.5 and 1.5 mm^2 active areas, obtained by etching away the ITO and Ge QD/SiO_2 layers using a dilute HCl solution. Current-voltage (*I–V*) measurements for the fabricated MOS photodetectors were carried out as a function of incident wavelength by illuminating the sample with a xenon lamp coupled to a spectrograph. The incident power at various wavelengths was measured using a calibrated power meter and it was kept constant at $P_{in}(\lambda) \sim 12\,\mu$W using a neutral density filter wheel. The *I–V* curves of two 1.5 mm^2 area Ge QD photodetectors, one fabricated by cleaving the original sample and the other defined by photolithography (see schematic in Fig. 1(a)), are presented in Fig. 1(b) at a representative incident wavelength of 600 nm. The PDs rectify in the dark with an on/off ratio greater than three orders of magnitude, measured at symmetric voltages of −1 and 1 V. They show a strong photoresponse (with photocurrent values three orders of magnitude higher than the dark current values for devices whose active area has been defined by photolithography) at −10 V and saturation below −7 V implying that they can be operated with almost unchanged performance in that voltage range. Most importantly, it is observed that the device defined by photolithography shows an order of magnitude decrease in dark current as a consequence of suppressed leakage on the periphery due to removal of the partially conducting Ge/SiO_2 matrix which is in contact with the Si substrate (see schematics in Fig. 1(a)). The 0.5 mm^2 devices also defined by photolithography exhibit even lower dark current of 6×10^{-9} A (not shown). The measured dark currents are about two orders of magnitude smaller compared to our previously reported photodetectors.[16,17] The mean values and standard deviation (presented as error bars) of the spectral responsivity (R_{sp}), external quantum efficiency (EQE) and internal quantum efficiency (IQE) of both pairs of identical area PDs are shown in Fig. 2 at a reverse bias of −10 V, together with the measured reflectance (R) at normal incidence, over the $\lambda = 400$–1100 nm wavelength range. The R_{sp}, EQE and R were determined using a QEX10 system from PV Measurements Inc. which includes a calibrated specular reflection reference sample and a calibrated silicon photodetector. The responsivity in Fig. 2(a) was measured by first calculating the photocurrent, i.e., $I_{ph} = |I_t - I_d|$, defined as the total current under illumination (I_t) minus the dark current (I_d) at the given reverse bias and incident wavelength (λ), and dividing it by the incident optical power, P_{in}, i.e.,

$$R_{sp}(\lambda) = \frac{I_{ph}(\lambda)}{P_{in}(\lambda)}. \quad (1)$$

As is evident in Fig. 2(a), the mean R_{sp} of the 0.5 mm^2 devices reaches a maximum of ~2 A/W, whereas that of the 1.5 mm^2 devices is ~1.7 A/W. The responsivity drops off as we approach the near ultraviolet and as well as near infrared but it is still ~0.3 A/W at 400 nm and 1100 nm, i.e., near the

a)S. Siontas and P. Liu contributed equally to this work.
b)Author to whom correspondence should be addressed. Electronic mail: Domenico_Pacifici@brown.edu.

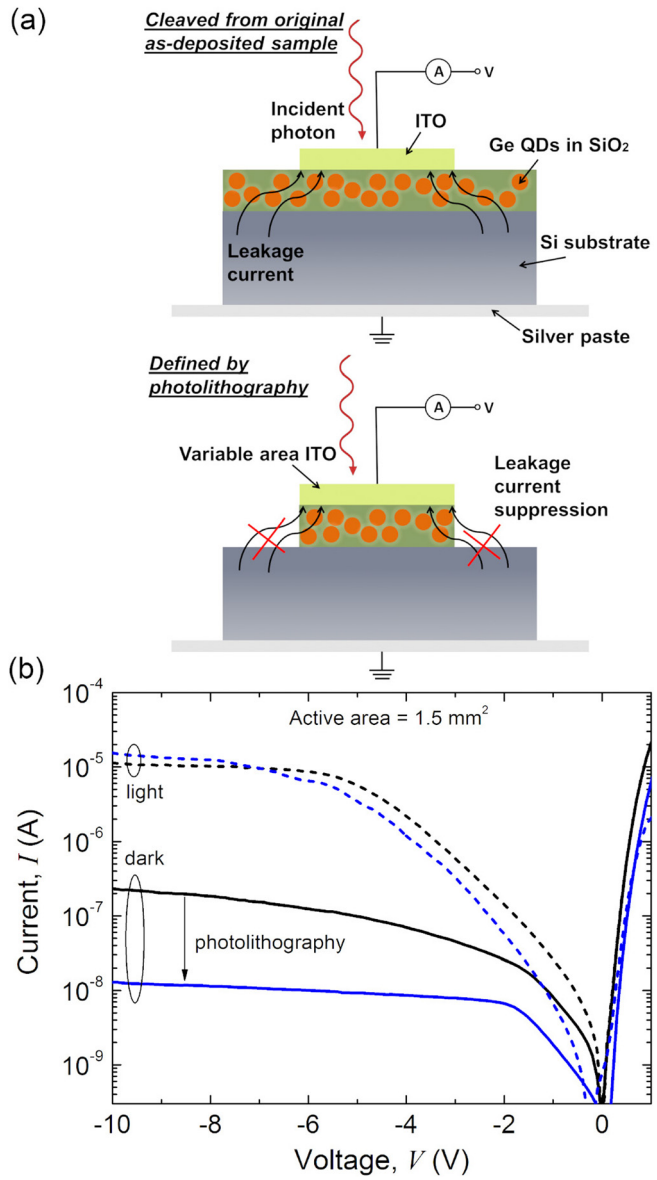

FIG. 1. (a) Schematic of the 1.5 mm^2 device, cleaved from the original sample, and a same size PD defined by photolithography. Arrows depict peripheral leakage current through the Ge/SiO_2 matrix. (b) Current-voltage characteristics showing the photoresponse of the two 1.5 mm^2 PDs as a function of reverse bias, in the dark and for incident light of $\lambda = 600$ nm at incident power equal to $\sim$12 μW. Black/blue solid lines depict dark current of cleaved/photolithographically defined sample, whereas dashed lines show current under illumination.

band-edge of the Si substrate. This is in contrast to the unannealed Ge QD PDs as published previously,[16,17] where R_{sp}, albeit possessing a higher peak value, goes to zero when the energy of the incident photon approaches the energy bandgap of silicon. The current devices exhibit a lower peak but a broader and more uniform spectral photoresponse. The extended spectral response can be explained by increased Ge QD size associated with an amorphous to crystalline phase transition,[6,13] leading to a smaller absorption bandgap, whereas absence of sharp absorption peaks is attributed to dispersion of QD sizes and an abundance of surface states.[15] Additionally, the low standard deviation of the mean R_{sp} for same area devices throughout all incident wavelengths (0.16 A/W for the 1.5 mm^2 and 0.1 A/W for the 0.5 mm^2 devices) is evidence that our fabrication process leads to reproducible results.

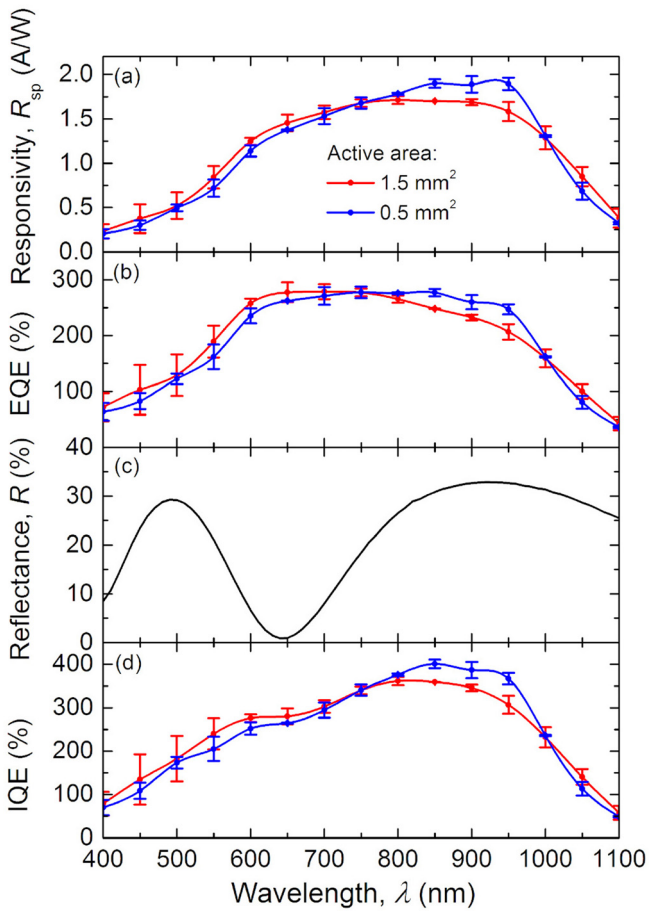

FIG. 2. (a) Responsivity R_{sp}, (b) external quantum efficiency EQE, (c) normal incidence reflectance R, and (d) internal quantum efficiency IQE spectra of the Ge QD photodetectors at reverse bias of -10 V. For panels (a), (b), and (d) each point represents the mean value, whereas the error bars represent the standard deviation of measurements performed on different devices with same area.

Moreover, R_{sp} values show little dependence on active area as the incident power density was kept constant during the measurements. The EQE of the PDs was also calculated as a function of λ by normalizing the photo-generated current by the number of incident photons at each wavelength, i.e.,

$$\mathrm{EQE}(\lambda) = \frac{I_{ph}(\lambda)}{P_{in}(\lambda)/E_{\gamma}(\lambda)}, \tag{2}$$

where $E_{\gamma}(\lambda)$ is the energy of a photon of free-space wavelength λ. The respective EQE curves of the detectors at reverse bias of -10 V are presented in Fig. 2(b). Both 0.5 and 1.5 mm^2 devices exhibit a mean peak value of $\sim$280%. In order to characterize the IQE, we measured the reflectance at normal incidence, shown in Fig. 2(c), and then normalized the number of photo-generated carriers by the number of absorbed photons, i.e., by $1 - R$ times the number of incident photons for any given λ, so that it is obtained by

$$\mathrm{IQE}(\lambda) = \frac{\mathrm{EQE}(\lambda)}{1 - R(\lambda)}. \tag{3}$$

Equation (3) assumes that all incident photons that are not reflected back into free space are absorbed in the PD active region comprising the Ge QD layer and the n-Si substrate

within a diffusion length of the Ge QD-containing interface. In reality, some photons may penetrate deeper into the substrate and create electron-hole pairs that recombine without contributing to the photocurrent, so the IQE estimated above, shown in Fig. 2(d), represents a lower bound on our PD performance. At -10 V of bias the mean peak IQE of the 0.5 mm^2 PDs reaches 400% whereas that of the 1.5 mm^2 devices is 360%. In agreement with Fig. 2(a), there is now a strong non-zero response near the Si band-edge, i.e., IQE $\sim$50% at $\lambda = 1100$ nm for both 1.5 and 0.5 mm^2 detectors, a remarkable result compared to previously reported data.[16,17] In addition to R_{sp} and IQE, the signal-to-noise ratio (SNR) is an important figure of merit for a photodetector, defined as SNR $= I_{ph}/\sigma_n$, where σ_n indicates the total current noise. In general, two main sources of noise need to be considered: the Poisson (shot) noise ($\sigma_s^2 = \sigma_{ph}^2 + \sigma_d^2 = 2e(I_{ph} + I_d)BG$) and the Johnson-Nyquist noise ($\sigma_j^2 = 4kTB/\mathcal{R}$), where σ_{ph} is the photocurrent shot noise, σ_d is the dark current shot noise, e is the elementary charge, I_d is the dark current, B is the -3 dB bandwidth, $kT = 0.026$ eV at room temperature, G is the internal gain (IQE), and $\mathcal{R}$ is the load resistance. In order to calculate SNR, we investigate the photocurrent, bandwidth and IQE dependence of the best performing 0.5 mm^2 device on incident power (measured using a calibrated power meter) at a reverse bias of -10 V. A 15 kΩ resistor connected in series to the PD acted as the load. The resistor value is far smaller than the effective PD's resistance so that the voltage drop across the PD approximately equals that of the biasing DC source. A 640 nm wavelength laser was used as an illumination source. Our obtained results are reported in Fig. 3. As demonstrated in Fig. 3(a), over the 10 nW to 12 μW range, I_{ph} increases linearly whereas the IQE remains approximately constant, showing only a slight increase at intermediate powers due to an increased charge (holes) trapping in the Ge QDs that causes a higher internal gain.[16] On the other hand, the -3 dB bandwidth B shows a sub-linear behavior, exhibiting a change of slope at $\sim$300 nW and reaching a maximum value of 2 kHz at 12 μW of incident power. The -3 dB bandwidth at each incident power was extracted from frequency dependent roll-off measurements of the peak to peak voltage drop across the load resistor, performed by direct digital modulation of the laser beam and is shown in the top inset of Fig. 3(c) for the representative 12 μW incident power case. Using the same experimental setup, we also studied the time response of the PDs as a function of area. As depicted in the bottom inset of Fig. 3(c), for a laser modulation frequency of 200 Hz the 0.5 mm^2 device shows a shorter rise time τ_r (130 μs) than the 1.5 mm^2 device (400 μs), therefore implying increased bandwidth. Specifically, the ratio of rise times approximately equals the ratio of device areas, suggesting that the smaller τ_r of the 0.5 mm^2 PD is a result of respective decrease of the $\mathcal{R}$C circuit constant. Considerably smaller response times, with slight effect on R_{sp}, can be achieved by thinning down the oxide layer as has been demonstrated previously.[17] In Fig. 4, we present the calculated noise current contributions to the total noise current and the respective room temperature SNR. As seen in Fig. 4(a), there is a clear crossover from the thermally dominated noise regime, defined as a total of the Johnson-Nyquist noise and the dark current shot noise,[18]

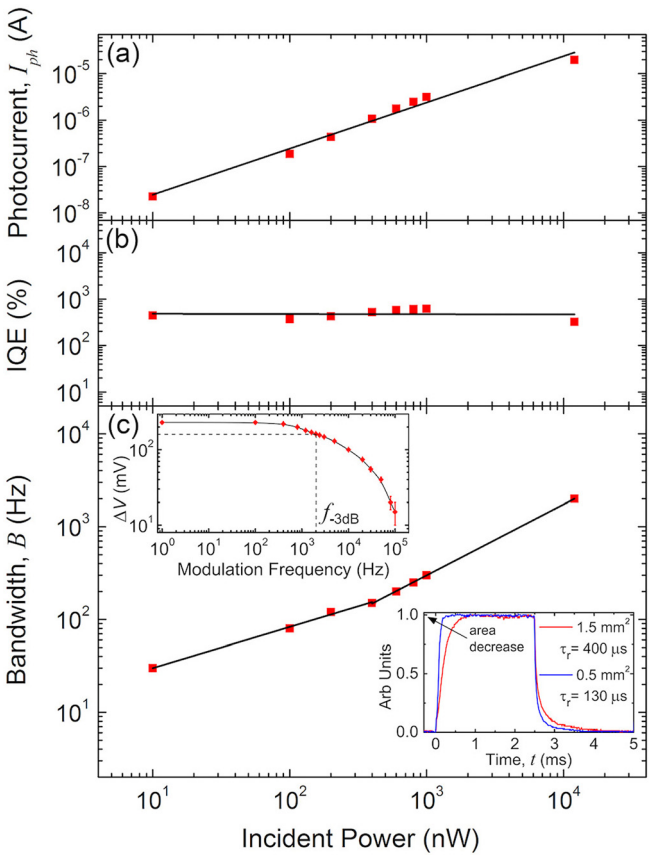

FIG. 3. Experimentally measured dependence of the (a) photocurrent, (b) IQE, and (c) bandwidth of the best performing 0.5 mm^2 Ge QD photodetector on incident optical power for reverse bias of -10 V. The top inset in panel (c) demonstrates the process of determining the -3 dB bandwidth B, i.e., carrying out frequency dependent roll off measurements, at a representative power of 12 μW. The bottom inset shows rise time measurements performed on a 0.5 mm^2 and 1.5 mm^2 area device inferring that the PDs' bandwidth scales inversely with area as a consequence of the reduced $\mathcal{R}$C constant.

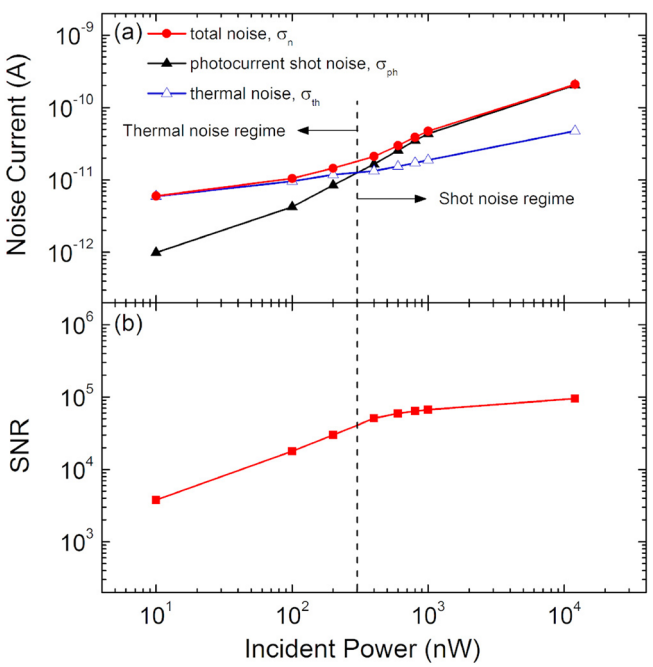

FIG. 4. (a) The two calculated main sources of noise current, showing crossover of the total noise from the thermal to the shot noise regime at $\sim$300 nW and (b) Signal-to-noise ratio of the best performing 0.5 mm^2 Ge QD photodetector at reverse bias of -10 V.

$\sigma_{th} = (\sigma_j^2 + \sigma_d^2)^{1/2}$, to the quantum regime dominated by the photocurrent shot noise, $\sigma_{ph} = (2eI_{ph}BG)^{1/2}$. The thermal noise dominates the low optical power range up to ~300 nW at which point the photocurrent shot noise σ_{ph} takes over. Having gathered full knowledge of the power dependence of each of the SNR components (I_{ph}, G, and B), the SNR is presented as a function of incident optical power in Fig. 4(b). Clearly, the SNR dependence on incident power comprises two distinct sub-linear regimes separated by a knee at ~300 nW. This behavior directly arises from the total noise σ_n being dominated by the thermal noise below 300 nW, where SNR can be approximated by $\mathrm{SNR} = I_{ph}/\sigma_{th}$, and by the photocurrent shot noise above 300 nW, where SNR is approximated by I_{ph}/σ_{ph}. Finally, Fig. 4(b) makes it possible to estimate the specific detectivity D^*, which is another basic figure of merit to assess the performance of photodetectors, defined as $D^* = (AB)^{1/2}/\mathrm{NEP}$, where A is the photodetector area and NEP is the noise-equivalent-power. NEP can be estimated by linearly extrapolating the thermally dominated range of the measured SNR from Fig. 4(b) to $\mathrm{SNR} = 1$, yielding NEP ~0.1 pW thus obtaining $D^* \simeq 6 \times 10^{12}$ cm $\mathrm{Hz}^{1/2}$ W^{-1}. Based on the measured R_{sp}, IQE, and D^*, the performance of Ge QD PDs is comparable to or higher than commercial Si photodetectors[19] and other photodetectors working in a similar spectral range,[20–27] as shown in Table S1.[28]

In summary, we have studied the photoresponse and noise performance of Ge QD MOS photodetectors on *n*-type Si substrates with various active areas defined by photolithography. Compared to previously reported data,[16,17] these devices exhibit reduced leakage current with consequently higher SNR and improved photoresponse near the edges of the 400–1100 nm spectral range. The results presented here demonstrate Ge QD photodetectors as promising alternatives to conventional silicon-based photodetectors.

This work was supported by the National Science Foundation under Grant No. DMR–1203186. The Brown University Microelectronics Central Facility and Harvard University CNS Facility are also gratefully acknowledged.

[1]L. Chen, P. Dong, and M. Lipson, Opt. Express **16**, 11513 (2008).
[2]L. Tang, S. E. Kocabas, S. Latif, A. K. Okyay, D.-S. Ly-Gagnon, K. C. Saraswat, and D. A. B. Miller, Nat. Photonics **2**, 226 (2008).
[3]V. Sorianello, A. De Iacovo, L. Colace, A. Fabbri, L. Tortora, E. Buffagni, and G. Assanto, Appl. Phys. Lett. **101**, 081101 (2012).
[4]M. Elkurdi, P. Boucaud, S. Sauvage, O. Kermarrec, Y. Campidelli, D. Bensahel, G. Saint-Girons, and I. Sagnes, Appl. Phys. Lett. **80**, 509 (2002).
[5]I. Stavarache, A.-M. Lepadatu, T. Stoica, and M. L. Ciurea, Appl. Surf. Sci. **285, Part B**, 175 (2013).
[6]C. Y. Chien, W. T. Lai, Y. J. Chang, C. C. Wang, M. H. Kuo, and P. W. Li, Nanoscale **6**, 5303 (2014).
[7]X. Liu, X. Ji, M. Liu, N. Liu, Z. Tao, Q. Dai, L. Wei, C. Li, X. Zhang, and B. Wang, ACS Appl. Mater. Interfaces **7**, 2452 (2015).
[8]M. H. Kuo, W. T. Lai, T. M. Hsu, Y. C. Chen, C. W. Chang, W. H. Chang, and P. W. Li, Nanotechnology **26**, 055203 (2015).
[9]Y. Itoh, S. Hatakeyama, T. Kawashima, and K. Washio, Thin Solid Films **602**, 32 (2016).
[10]J.-M. Shieh, Y.-F. Lai, W.-X. Ni, H.-C. Kuo, C.-Y. Fang, J. Y. Huang, and C.-L. Pan, Appl. Phys. Lett. **90**, 051105 (2007).
[11]M. Fujii, O. Mamezaki, S. Hayashi, and K. Yamamoto, J. Appl. Phys. **83**, 1507 (1998).
[12]B. Zhang, S. Shrestha, M. A. Green, and G. Conibeer, Appl. Phys. Lett. **96**, 261901 (2010).
[13]S. Cosentino, S. Mirabella, M. Miritello, G. Nicotra, R. L. Savio, F. Simone, C. Spinella, and A. Terrasi, Nanoscale Res. Lett. **6**, 135 (2011).
[14]C. Palade, A.-M. Lepadatu, I. Stavarache, V. Teodorescu, and M. Ciurea, in *2013 International* Semiconductor Conference (CAS) (2013), Vol. 1, pp. 31–34.
[15]S. Cosentino, E. Barbagiovanni, I. Crupi, M. Miritello, G. Nicotra, C. Spinella, D. Pacifici, S. Mirabella, and A. Terrasi, Sol. Energy Mater. Sol. Cells **135**, 22 (2015).
[16]S. Cosentino, P. Liu, S. T. Le, S. Lee, D. Paine, A. Zaslavsky, D. Pacifici, S. Mirabella, M. Miritello, I. Crupi, and A. Terrasi, Appl. Phys. Lett. **98**, 221107 (2011).
[17]P. Liu, S. Cosentino, S. T. Le, S. Lee, D. Paine, A. Zaslavsky, D. Pacifici, S. Mirabella, M. Miritello, I. Crupi, and A. Terrasi, J. Appl. Phys. **112**, 083103 (2012).
[18]S. Donati, *Photodetectors: Devices, Circuits, and Applications* (Prentice Hall PTR, 2000).
[19]See https://www.thorlabs.com/ for "Biased Si detectors 200–1100 nm".
[20]M. Razeghi and A. Rogalski, J. Appl. Phys. **79**, 7433 (1996).
[21]S. A. Mcdonald, G. Konstantatos, S. Zhang, P. W. Cyr, E. J. Klem, L. Levina, and E. H. Sargent, Nat. Mater. **4**, 138 (2005).
[22]G. Konstantatos, I. Howard, A. Fischer, S. Hoogland, J. Clifford, E. Klem, L. Levina, and E. H. Sargent, Nature **442**, 180 (2006).
[23]M. Sofos, J. Goldberger, D. A. Stone, J. E. Allen, Q. Ma, D. J. Herman, W.-W. Tsai, L. J. Lauhon, and S. I. Stupp, Nat. Mater. **8**, 68 (2009).
[24]X. Gong, M. Tong, Y. Xia, W. Cai, J. S. Moon, Y. Cao, G. Yu, C.-L. Shieh, B. Nilsson, and A. J. Heeger, Science **325**, 1665 (2009).
[25]X. Gong, M.-H. Tong, S. H. Park, M. Liu, A. Jen, and A. J. Heeger, Sensors **10**, 6488 (2010).
[26]L. Li, Y. Huang, J. Peng, Y. Cao, and X. Peng, J. Mater. Chem. C **2**, 1372 (2014).
[27]X. Li, M. Zhu, M. Du, Z. Lv, L. Zhang, Y. Li, Y. Yang, T. Yang, X. Li, K. Wang, H. Zhu, and Y. Fang, Small **12**, 549 (2016).
[28]See supplementary material at http://dx.doi.org/10.1063/1.4960532 for a table comparing the performance and figures of merit of several photodetectors based on published data.